Super-Resonant Transport of Topological Surface States Subjected to In-Plane Magnetic Fields

Song-Bo Zhang[1,*] Chang-An Li,[1] Francisco Peña-Benitez[2,3] Piotr Surówka[2,3,4] Roderich Moessner,[2,3] Laurens W. Molenkamp,[5,6,3,7] and Björn Trauzettel[1,3]

[1]*Institut für Theoretische Physik und Astrophysik, Universität Würzburg, 97074 Würzburg, Germany*
[2]*Max-Planck-Institut für Physik komplexer Systeme, Nöthnitzer Strasse 38, 01187 Dresden, Germany*
[3]*Würzburg-Dresden Cluster of Excellence ct.qmat, Germany*
[4]*Department of Theoretical Physics, Wrocław University of Science and Technology, 50-370 Wrocław, Poland*
[5]*Physikalisches Institut (EP3), Universität Würzburg, Am Hubland, 97074 Würzburg, Germany*
[6]*Institute for Topological Insulators, Universität Würzburg, Am Hubland, 97074 Würzburg, Germany*
[7]*Max Planck Institute for Chemical Physics of Solids, D-01187 Dresden, Germany*

(Received 26 February 2021; revised 19 April 2021; accepted 13 July 2021; published 10 August 2021)

Magnetic oscillations of Dirac surface states of topological insulators are typically expected to be associated with the formation of Landau levels or the Aharonov-Bohm effect. We instead study the conductance of Dirac surface states subjected to an in-plane magnetic field in the presence of a barrier potential. Strikingly, we find that, in the case of large barrier potentials, the surface states exhibit pronounced oscillations in the conductance when varying the magnetic field, in the *absence* of Landau levels or the Aharonov-Bohm effect. These novel magnetic oscillations are attributed to the emergence of *super-resonant transport* by tuning the magnetic field, in which many propagating modes cross the barrier with perfect transmission. In the case of small and moderate barrier potentials, we identify a positive magnetoconductance due to the increase of the Fermi surface by tilting the surface Dirac cone. Moreover, we show that for weak magnetic fields, the conductance displays a shifted sinusoidal dependence on the field direction with period π and phase shift determined by the tilting direction with respect to the field direction. Our predictions can be applied to various topological insulators, such as HgTe and Bi_2Se_3, and provide important insights into exploring and understanding exotic magnetotransport properties of topological surface states.

DOI: 10.1103/PhysRevLett.127.076601

Introduction.—Topological insulators host gapless surface states which stem from nontrivial bulk topology [1–3]. These surface states can be modeled by a single Dirac cone. Over the last two decades, topological insulators have been discovered in numerous materials [4–12] including HgTe [13], $Bi_{1-x}Sb_x$ [14], and Bi_2Se_3 [15–18]. Magnetotransport of Dirac surface states has been an active research topic [19–51], theoretically and experimentally, since the discovery of topological insulators. It provides vital features, which include particularly magnetic oscillations, to detect and characterize Dirac surface states. Magnetic oscillations are usually associated with the formation of Landau levels or the Aharonov-Bohm effect [19–24,33–38]. Thus, a fundamentally intriguing question is whether magnetic oscillations of topological surface states can appear in the absence of Landau levels or the Aharonov-Bohm effect. In slab geometries of topological insulators, in-plane magnetic oscillations as a function of field strength are oftentimes observed [44,52,53]. To the best of our knowledge, a convincing explanation of these oscillations is still lacking.

Notably, in typical topological insulators, electron-hole symmetry in the energy spectrum of surface states is broken by the presence of higher-order momentum corrections [54–56]. To fully understand the transport properties of surface states in realistic systems, the consideration of this electron-hole asymmetry is important. Interestingly, the interplay of electron-hole asymmetry and in-plane magnetic fields tilts the surface states at low energies [50].

In this Letter, we study the conductance of topological surface states in the presence of a barrier potential and external in-plane magnetic fields, taking into account the electron-hole asymmetry of the energy spectrum. We find that for small and moderate barrier potentials (comparable to the Fermi energy), the surface states exhibit a positive magnetoconductance due to the increase of the Fermi surface by tilting in any direction. Remarkably, for larger barrier potentials, super-resonant transport of surface states appears by tuning the magnetic field, which enables many surface propagating modes to tunnel through the barrier without backscattering. This super-resonant transport results in pronounced oscillations in the conductance as strength or direction of the magnetic field are varied. Moreover, we show that for moderate magnetic fields, the conductance is a sinusoidal function of field direction with period π and phase shift dependent on the angle

between tilting and field directions. Our predictions are applicable to a variety of topological insulators including HgTe and Bi_2Se_3.

Effective Hamiltonian of surface states.—The states of a topological insulator on a surface can be described by a single Dirac cone [15,54,55],

$$H(\mathbf{k}) = m\mathbf{k}^2 + v(k_x s_y - k_y s_x), \tag{1}$$

where $\mathbf{k} = (k_x, k_y)$ are momenta in the vicinity of the Γ point, v is the Fermi velocity, and s_x and s_y are Pauli matrices acting on spin space. Moreover, in certain topological insulators, for instance, HgTe with zinc-blende crystal structure, bulk inversion symmetry is broken, leading to extra terms $H_{\mathrm{BIA}} = v_b(k_x s_x + k_y s_y) + \gamma k_x k_y$ [57]. Note that we have included the quadratic terms in momentum $m\mathbf{k}^2$ and $\gamma k_x k_y$, which preserve time-reversal symmetry. These terms are often ignored in previous studies for simplicity [65]. However, they break electron-hole symmetry in the energy spectrum and can lead to interesting physics as we show below.

Applying an in-plane magnetic field $\mathbf{B} = B(\cos\theta, \sin\theta)$ introduces a Zeeman term $H_Z = g\mu_B \mathbf{B}\cdot\mathbf{s}/2$, where g is the g factor, μ_B is the Bohr magneton, and B and θ denote the strength and direction of the magnetic field, respectively. The Zeeman term not only shifts the Dirac cone away from the Γ point in momentum space but also tilts the Dirac cone [50]. Considering that v_b is typically much smaller than v [66], we can find the position shift of the Dirac point as $\mathbf{k}_s = k_s(-\sin\theta, \cos\theta)$, with $k_s = g\mu_B B/2v$. Near the Dirac point, the effective model for surface states can be written as [57]

$$\mathcal{H}(\mathbf{k}) = v(\tilde{k}_x s_y - \tilde{k}_y s_x) + t_x\tilde{k}_x + t_y\tilde{k}_y, \tag{2}$$

where $\tilde{\mathbf{k}} = \mathbf{k} - \mathbf{k}_s$, and the tilting vector $\mathbf{t} \equiv (t_x, t_y)$ is given by

$$\mathbf{t} = k_s(\gamma\cos\theta - 2m\sin\theta, 2m\cos\theta - \gamma\sin\theta). \tag{3}$$

The eigenenergies are tilted as $E_\pm(\mathbf{k}) = \mathbf{t}\cdot\tilde{\mathbf{k}} \pm v|\tilde{\mathbf{k}}|$. The tilting strength $|\mathbf{t}|$ is proportional to the field strength, and the tilting direction is controllable by the field direction. We focus on the realistic case with small tilting $|\mathbf{t}| < |v|$ throughout.

Transmission probability.—We consider the surface states with a barrier potential V_0 extending over a length of L in the x direction, as sketched in Fig. 1. The in-plane magnetic field is applied to the whole system. This setup can be described by

$$\mathcal{H}_{\mathrm{tot}} = \mathcal{H}(-i\partial_{\mathbf{r}}) - E_F + V(x), \tag{4}$$

with E_F as the Fermi energy, and the local electronic potential $V(x) = V_0$ for $|x| \leq L/2$ and 0 otherwise [67].

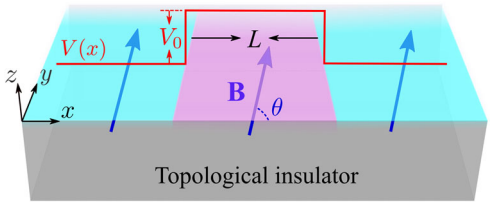

FIG. 1. Schematic of surface states (cyan and magenta) of a topological insulator (gray) with a barrier potential V_0 extending over a length of L. An in-plane magnetic field $\mathbf{B}$ (blue arrows) is applied to the system.

V_0 can be created by local gating [69]. It can be positive or negative. For simplicity, we assume the system to be large in the y direction such that the transverse momentum k_y is conserved.

To study the transport properties of the system, we employ the scattering approach. In each region, we find two eigenstates for given k_y and energy E. In the regions away from the barrier, their wave functions can be written as

$$\psi_\pm(x,y) = e^{i\tilde{k}_y y} e^{i\tilde{k}_\pm x}(\, e^{i\theta_\pm}, -1\,)^T/\mathcal{N}_\pm, \tag{5}$$

where $e^{i\theta_\pm} \equiv v(\tilde{k}_y + i\tilde{k}_\pm)/(E_{k_y} - t_x\tilde{k}_\pm)$, $E_{k_y} = E + E_F - t_y\tilde{k}_y$, $\mathcal{N}_\pm = \sqrt{1 + |e^{i\theta_\pm}|^2}$, and the wave numbers $\tilde{k}_\pm$ in the x direction read as

$$\tilde{k}_\pm = \left[-t_x E_{k_y} \pm v\sqrt{E_{k_y}^2 - (v^2 - t_x^2)\tilde{k}_y^2}\,\right] \Big/ (v^2 - t_x^2). \tag{6}$$

In the barrier region, the wave functions have the same form as Eq. (5) but with E_{k_y} replaced by $E^B_{k_y} = E_{k_y} - V_0$. Correspondingly, we use superscript B to indicate the angles $\theta^B_\pm$ and wave numbers $\tilde{k}^B_\pm$ inside the barrier region.

The scattering state of injecting an electron from the one lead to the junction can be expanded in terms of the basis wave functions, Eq. (5). Matching the wave function of the scattering state at the interfaces, we derive the transmission coefficient as

$$t_{\tilde{k}_y} = e^{-i\tilde{k}_+ L} e^{i(\tilde{k}^B_- + \tilde{k}^B_+)L}(e^{i\theta_+} - e^{i\theta_-})(e^{i\theta^B_+} - e^{i\theta^B_-})/\mathcal{Z}, \tag{7}$$

where $\mathcal{Z} = e^{i\tilde{k}^B_+ L}(e^{i\theta_+} - e^{i\theta^B_+})(e^{i\theta_-} - e^{i\theta^B_-}) - e^{i\tilde{k}^B_- L}(e^{i\theta_+} - e^{i\theta^B_-})(e^{i\theta_-} - e^{i\theta^B_+})$ [70]. The transmission probability is then given by $T_{\tilde{k}_y} = |t_{\tilde{k}_y}|^2$. More details of the derivation are presented in the Supplemental Material [57]. For the incident modes with $\tilde{k}_y = 0$, we always have $\theta_\pm = \theta^B_\pm = \pm\pi/2$ and hence $T_{\tilde{k}_y=0} = 1$. This perfect transmission results from spin conservation and is related to Klein tunneling [58]. Notably, without tilting, the results are independent of the magnetic field. This indicates that a simple position shift of the Dirac cone in momentum space does not change the transport properties of surface states.

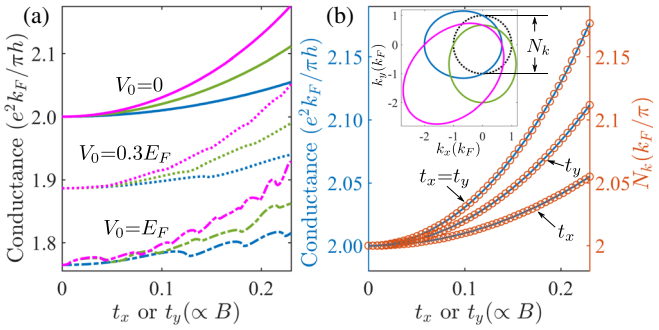

FIG. 2. (a) Conductance G (in units of $e^2k_F/\pi h$ with $k_F=|E_F/v|$) as a function of tilt strength t_x (for $t_y=0$, blue), t_y (for $t_x=0$, green), and $t_x=t_y=t$ (magenta) for $E_F=100v/L$ and $V_0=0$ (solid), $0.3E_F$ (dotted), and E_F (broken), respectively. (b) Number N_k of propagating modes (in units of k_F/π) as a function of t_x (for $t_y=0$), t_y (for $t_x=0$), and $t_x=t_y=t$, respectively. Inset: Fermi surfaces for $\mathbf{t}=(0.5,0)v$, $(0,0.5)v$, and $(0.5,0.5)v$.

Positive magnetoconductance.—With the transmission probability, the (differential) conductance G (per unit length) at zero temperature and zero bias voltage can be evaluated as

$$G=\frac{e^2}{h}\int\frac{d\tilde{k}_y}{2\pi}T_{\tilde{k}_y}(E=0), \tag{8}$$

where the sum runs over all modes distinguished by $\tilde{k}_y$.

We first look at the case of small and moderate barrier potentials, i.e., $|V_0|\lesssim|E_F|$, as shown in Fig. 2. Notably, G increases as we increase the tilting strength in any direction. Recalling that the tilting strength grows linearly with increasing magnetic field B, this indicates a positive magnetoconductance. For small barrier potentials, $|V_0|\ll|E_F|$, G increases monotonically with increasing B. A larger barrier potential suppresses G and induces slight oscillations. However, G increases overall, with increasing B [Fig. 2(a)]. These oscillations are closely related to the super-resonant transport of tilted surface electrons, which we discuss later.

The positive magnetoconductance can be attributed to the enhanced Fermi surface of tilted surface states. To understand this, it is instructive to consider the zero-barrier limit $V_0=0$. In this limit, all propagating modes transmit through the junction without reflection. Thus, the conductance is simply given by the number N_k of propagating modes, i.e., $G=(e^2/h)N_k$. N_k is determined by the size of the Fermi surface in the k_y direction, as illustrated in the inset of Fig. 2(b). Tilting the surface Dirac cone in any direction enlarges the Fermi surface and hence the number of propagating modes. As shown by the circles in Fig. 2(b), we calculate N_k numerically as a function of the tilting strength in three different directions as considered in Fig. 2(a). Evidently, this dependence nicely agrees with the magnetoconductance (solid curves). When the tilting occurs in the x or y direction, we can find N_k analytically from the tilted spectrum. Namely, $N_k=|E_F|/(\pi\sqrt{v^2-t_x^2})$ for tilting in the x direction, and $N_k=|vE_F|/[\pi(v^2-t_y^2)]$ for tilting in the y direction.

Super-resonant transport and conductance oscillations.—Now, we consider larger barrier potentials, $|V_0|>|E_F|$, and analyze the magnetic oscillations of the conductance. These oscillations can be understood as the emergence of super-resonant (transport) regimes of surface states, where many propagating modes perfectly transmit through the barrier at the same magnetic field (i.e., the same tilting). To make this clearer and simplify the analysis, we first focus on the large barrier limit, $|V_0|\gg|E_F|$. In this limit, we can approximate $\theta_\pm^B\approx\pm\pi/2$ in Eq. (7) and simplify

$$T_{\tilde{k}_y}=\frac{1-\cos(\theta_+-\theta_-)}{1-\sin\theta_+\sin\theta_--\cos[(\tilde{k}_+^B-\tilde{k}_-^B)L]\cos\theta_+\cos\theta_-}. \tag{9}$$

From this expression [more generally Eq. (7)], we find that the barrier becomes transparent for the mode with index $\tilde{k}_y$ when the resonance condition, $\sin[(\tilde{k}_+^B-\tilde{k}_-^B)L/2]=0$, is fulfilled. Using the expressions for $\tilde{k}_\pm^B$ in Eq. (6), the resonance condition reads explicitly as

$$(V_0-t_y\tilde{k}_y)^2-(v^2-t_x^2)\tilde{k}_y^2=[n\pi(v^2-t_x^2)/(vL)]^2 \tag{10}$$

with n an integer. This means that an electron acquires a phase shift $2n\pi$ in one round trip between the interfaces [71].

When the tilting is in the junction (i.e., x) direction, we find the solutions of t_x to Eq. (10) as

$$t_x\approx\pm\sqrt{v^2-|vV_0|L/\pi n} \tag{11}$$

for integers $n>|V_0L/\pi v|$. Strikingly, these solutions are independent of the mode index $\tilde{k}_y$ [72]. This indicates the super-resonant regimes where all propagating modes with different $\tilde{k}_y$ exhibit perfect transmission. As a result, we observe resonance peaks in $T_{\tilde{k}_y}$ and thus the maximal conductance $G_{\max}=(e^2/h)N_k$ at t_x $(\propto B)$ determined by Eq. (11). Moreover, we find that at $t_x=\pm\sqrt{v^2-|vV_0|L/[\pi(n+1/2)]}$, all modes have instead the lowest transmission probabilities given by $T_{\tilde{k}_y}=1-(v^2-t_x^2)\tilde{k}_y^2/E_F^2$ [57]. Summing over all modes, we obtain the minimal conductance as $G_{\min}=(2e^2/3h)N_k$. Therefore, we observe pronounced oscillations of G with magnitude $\Delta G_{\rm osc}$ as large as one third of the maximal conductance:

$$\Delta G_{\rm osc}=G_{\max}/3. \tag{12}$$

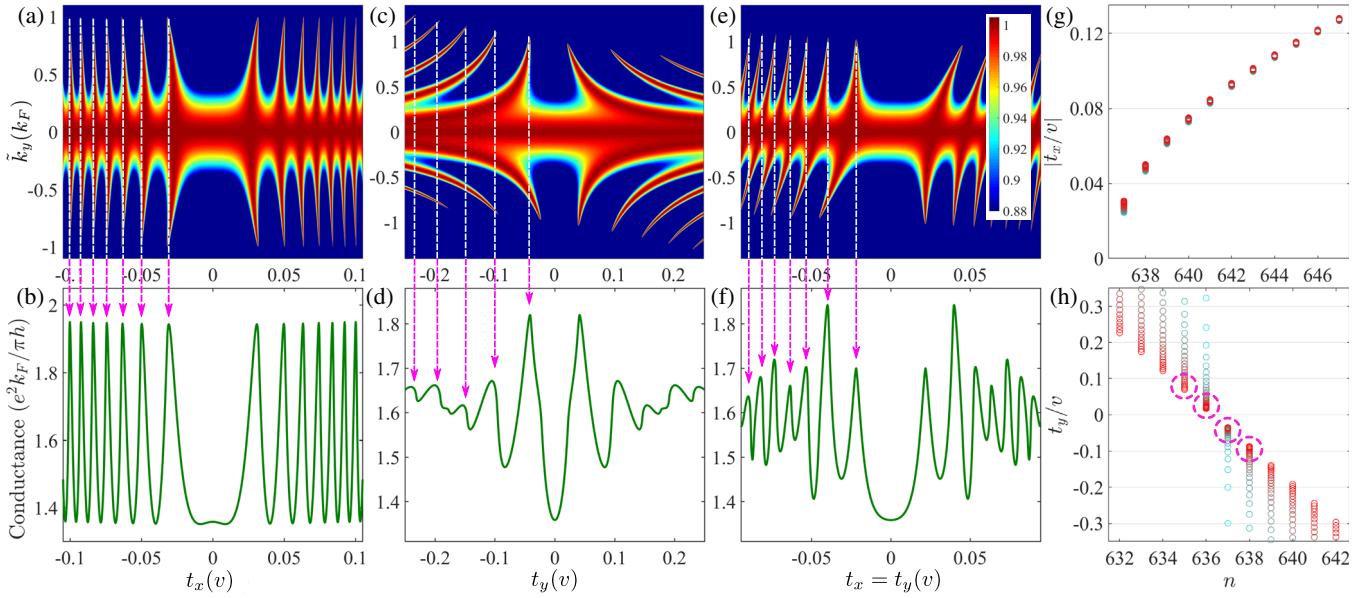

FIG. 3. (a) Transmission probability density against $\tilde{k}_y$ and t_x for $t_y = 0$. (b) Conductance G as a function of t_x for $t_y = 0$. (c) Transmission probability density against $\tilde{k}_y$ and t_y for $t_x = 0$. (d) G as a function of t_y for $t_x = 0$. (e) Transmission probability density against $\tilde{k}_y$ and $t_x = t_y = t$. (f) G as a function of $t_x = t_y = t$. In (b), (d) and (e), the peaks (marked by magenta arrows) of G correspond to the super-resonant regimes. (g) Solutions of t_x to Eq. (10) for $t_y = 0$ and different integers n and mode indices $\tilde{k}_y$. (h) Solutions of t_y to Eq. (10) for $t_x = 0$ and different n and $\tilde{k}_y$. In (g) and (h), the color changes from cyan to red when $\tilde{k}_y$ increases from 0 to $1.2k_F$. In (h), the super-resonant regimes are marked by the dashed circles. Other parameters are $E_F = vk_F = 50v/L$ and $V_0 = 40E_F$. We provide more illustrations for other values of V_0 in the Supplemental Material [57].

Interestingly, the values of $G_{\max}$, $G_{\min}$, and $\Delta G_{\rm osc}$ (in units of N_k) are universal and independent of the potential V_0 and length L of the barrier [73]. Considering the increase of N_k, when strengthening B, $\Delta G_{\rm osc}$ increases. In contrast, according to Eq. (11), the separations between the conductance peaks depend strongly on the product V_0L, whereas they are insensitive to E_F. Moreover, they decrease with increasing B. All these results are in accordance with our numerical results displayed in Figs. 3(a), 3(b), and 3(g).

When the tilting is in the transverse (i.e., y) direction, the solutions to Eq. (10) are given by $t_y = V_0/\tilde{k}_y - v\sqrt{1 + (\pi n/\tilde{k}_y L)^2}$. For n close to $n_c \equiv [|V_0L/\pi v|]$, the greatest integer less than $|V_0L/\pi v|$, we find that most of the propagating modes exhibit a resonance condition at

$$t_y \approx \pm(|vV_0|L - \pi n v^2)/|E_F L|. \tag{13}$$

Hence, in this tilting direction, we also observe the resonance peaks and pronounced oscillations in the conductance [Fig. 3(d)]. In contrast with the case with tilting in the junction direction, the separations between the conductance peaks are sensitive not only to L and V_0 individually, but also to E_F. Moreover, Eq. (13) indicates that the separations between the conductance peaks are almost constant with respect to B. However, as B increases, the resonance positions for different propagating modes become more extended [Figs. 3(c) and 3(h)]. Consequently, the magnitude of oscillations is strongest for small B but suppressed for large B.

For the general case with the tilting direction deviating from the x and y directions, $t_x = \varepsilon t_y$ with $\varepsilon \neq 0$, we can also observe magnetoconductance oscillations [Figs. 3(e) and 3(f)]. These oscillations can be similarly attributed to the super-resonant transport of surface states as varying B. However, they are less regular, compared with the two special cases discussed above. The oscillations are aperiodic in B, and the positions of the peaks become hard to predict in general.

Note that although we focus on the large barrier limit in the above analysis, the conductance oscillations remain pronounced even when the barrier potential is of the same order as the Fermi energy, $|V_0| \gtrsim |E_F|$ [see Fig. 2(a) and Sec. VI in the Supplemental Material [57]].

Dependence on field direction.—As we have discussed before, the conductance G depends on the tilting direction which, in turn, is determined periodically by the field direction θ, according to Eq. (3). Therefore, G depends periodically on θ. This field-direction dependence stems from two origins: (i) the anisotropic Fermi surface and (ii) the barrier transparency for conducting channels. In Fig. 4, we calculate numerically G as a function of θ. Several interesting features can be observed.

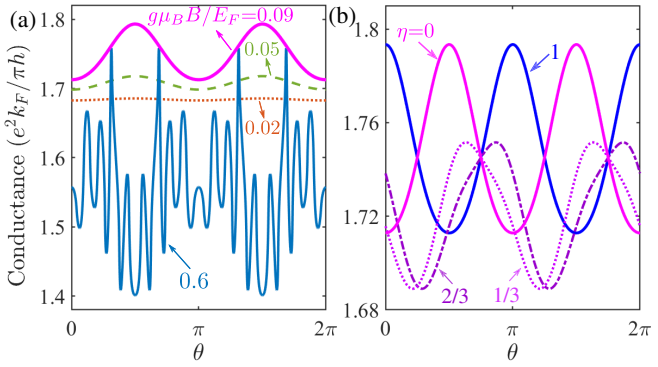

FIG. 4. (a) Conductance G as a function of field direction θ for $m = 10^{-3}vL$, $\gamma = 0$, and $g\mu_B B = 0.02E_F$, $0.05E_F$, $0.09E_F$, and $0.6E_F$, respectively. (b) The same as (a) but for $g\mu_B B = 0.02E_F$, $m = 10^{-3}(1-\eta)vL$, and $\gamma = 2\times 10^{-3}\eta vL$ with $\eta = 0$, $1/3$, $2/3$, and 1 (from magenta to blue), respectively. Other parameters are $E_F = 100v/L$ and $V_0 = 40E_F$.

First, G has a period of π in θ. For small field strengths $B < B_c$, $G(\theta)$ displays approximately a sinusoidal dependence, $G(\theta) - G_0 \propto \sin[2(\theta-\theta_0)]$, where G_0 is a (θ-independent) constant and B_c corresponds to the field strength at which the first conductance peak is located [74]. If the tilting direction is parallel ($m = 0$) or perpendicular ($\gamma = 0$) to the field direction, the phase shift becomes $\theta_0 = 0$ or $\pi/2$. However, if the tilting direction is neither parallel nor perpendicular to the field direction ($m\gamma \neq 0$), then θ_0 is different from 0 and $\pi/2$ [Fig. 4(b)]. Second, if we increase the field strength B, the dependence on θ becomes more pronounced [Fig. 4(a)]. This shows that the anisotropy of surface states is enhanced by increasing B via the tilting effect. Third, for stronger field strengths $B > B_c$, G oscillates with a number of peaks and valleys in one period $\theta \in [0,\pi)$ (blue curve). These dense oscillations with respect to θ can also be related to the super-resonant transport of surface states analyzed before. It is interesting to note that clear field-direction dependence in the resistance of topological surface states has been observed recently [44,52].

Conclusion and discussion.—We have identified a positive magnetoconductance of topological surface states, which stems from the increase of the Fermi surface by applying in-plane magnetic fields. We have unveiled the super-resonant transport of the surface states by tuning the magnetic field, which enables many propagating modes to transmit a barrier potential without backscattering. This super-resonant transport results in pronounced oscillations in the magnetoconductance.

We note that the appearance of the positive magnetoconductance and conductance oscillations can be directly attributed to the deformation of the surface Dirac cone by in-plane magnetic fields. In this work, the crucial role of deforming is played by tilting the Dirac cone via the Zeeman effect. Particularly, the anomalous conductance oscillations arising from the super-resonant transport of surface states are essentially different from conventional magnetic oscillations, which typically stem from the formation of Landau levels or the Aharonov-Bohm effect.

Our predictions can be implemented in various candidate materials including HgTe and Bi_2Se_3 where in-plane magnetic fields have been successfully applied to surface states [27,44,52,75–78]. Consider HgTe with parameters $v = 256\,\text{meV}\cdot\text{nm}$, $m = 108\,\text{meV}\cdot\text{nm}^2$, $\gamma = -64\,\text{meV}\cdot\text{nm}^2$, $g = 20$ [57], $L = 2\ \mu\text{m}$, and $V_0 = 40$ meV [79]. We could observe magnetic oscillations for tilting $t_c > v\sqrt{1 - V_0 L/[\pi v(n_c + 1/2)]} \simeq 0.017v$ and thus for magnetic fields $B > 2t_c v/(g\mu_B\sqrt{4m^2+\gamma^2}) \simeq 8.4$ T. For Bi_2Se_3 with $v = 330\,\text{meV}\cdot\text{nm}$, $m = 237\,\text{meV}\cdot\text{nm}^2$, $\gamma = 0$, $g = 19.4$, $L = 2\ \mu\text{m}$, and $V_0 = 150$ meV [57], we could observe the oscillations for $B > 8.6$ T [84].

We thank Abu Aravindnath, Mohamed AbdelGhany, Wouter Beugeling, Hartmut Buhmann, Charles Gould, and Benedikt Mayer for valuable discussions. This work was supported by the DFG [SPP1666, SFB1170 "ToCoTronics," and SFB1143 (Project No. 247310070)], the Würzburg-Dresden Cluster of Excellence ct.qmat (EXC2147, Project No. 390858490), and the Elitenetzwerk Bayern Graduate School on "Topological Insulators." P. S. is also supported by the DFG through the Leibniz Program and the National Science Centre Sonata Bis, Grant No. 2019/34/E/ST3/00405.

*songbo.zhang@physik.uni-wuerzburg.de

[1] M. Z. Hasan and C. L. Kane, Colloquium: Topological insulators, Rev. Mod. Phys. **82**, 3045 (2010).
[2] X. L. Qi and S. C. Zhang, Topological insulators and superconductors, Rev. Mod. Phys. **83**, 1057 (2011).
[3] S.-Q. Shen, *Topological Insulators: Dirac Equation in Condensed Matters* (Springer, Berlin, 2012).
[4] L. Fu and C. L. Kane, Topological insulators with inversion symmetry, Phys. Rev. B **76**, 045302 (2007).
[5] T. Sato, K. Segawa, H. Guo, K. Sugawara, S. Souma, T. Takahashi, and Y. Ando, Direct Evidence for the Dirac-Cone Topological Surface States in the Ternary Chalcogenide $TlBiSe_2$, Phys. Rev. Lett. **105**, 136802 (2010).
[6] M. Z. Hasan and J. E. Moore, Three-dimensional topological insulators, Annu. Rev. Condens. Matter Phys. **2**, 55 (2011).
[7] Y. Tanaka, Z. Ren, T. Sato, K. Nakayama, S. Souma, T. Takahashi, K. Segawa, and Y. Ando, Experimental realization of a topological crystalline insulator in SnTe, Nat. Phys. **8**, 800 (2012).
[8] S.-Y. Xu, C. Liu, N. Alidoust, M. Neupane, D. Qian, I. Belopolski *et al.*, Observation of a topological crystalline insulator phase and topological phase transition in Pb_xSn_xTe, Nat. Commun. **3**, 1192 (2012).
[9] T. H. Hsieh, H. Lin, J. Liu, W. Duan, A. Bansil, and L. Fu, Topological crystalline insulators in the SnTe material class, Nat. Commun. **3**, 982 (2012).

[10] P. Dziawa, B. J. Kowalski, K. Dybko, R. Buczko, A. Szczerbakow, M. Szot *et al.*, Topological crystalline insulator states in $Pb_{1-x}Sn_xSe$, Nat. Mater. **11**, 1023 (2012).
[11] B. Yan and S. C. Zhang, Topological materials, Rep. Prog. Phys. **75**, 096501 (2012).
[12] Y. Ando, Topological insulator materials, J. Phys. Soc. Jpn. **82**, 102001 (2013).
[13] C. Brüne, C. X. Liu, E. G. Novik, E. M. Hankiewicz, H. Buhmann, Y. L. Chen, X. L. Qi, Z. X. Shen, S. C. Zhang, and L. W. Molenkamp, Quantum Hall Effect from the Topological Surface States of Strained Bulk HgTe, Phys. Rev. Lett. **106**, 126803 (2011).
[14] D. Hsieh, D. Qian, L. Wray, Y. Xia, Y. S. Hor, R. J. Cava, and M. Z. Hasan, A topological Dirac insulator in a quantum spin Hall phase, Nature (London) **452**, 970 (2008).
[15] H. Zhang, C. X. Liu, X. L. Qi, X. Dai, Z. Fang, and S. C. Zhang, Topological insulators in Bi_2Se_3, Bi_2Te_3 and Sb_2Te_3 with a single Dirac cone on the surface, Nat. Phys. **5**, 438 (2009).
[16] Y. L. Chen, J. G. Analytis, J. H. Chu, Z. K. Liu, S. K. Mo, X. L. Qi *et al.*, Experimental realization of a three-dimensional topological insulator, Bi_2Te_3, Science **325**, 178 (2009).
[17] D. Hsieh, Y. Xia, D. Qian, L. Wray, F. Meier, J. H. Dil *et al.*, Observation of Time-Reversal-Protected Single-Dirac-Cone Topological-Insulator States in Bi_2Te_3 and Sb_2Te_3, Phys. Rev. Lett. **103**, 146401 (2009).
[18] Y. Xia, D. Qian, D. Hsieh, L. Wray, A. Pal, H. Lin *et al.*, Observation of a large-gap topological-insulator class with a single Dirac cone on the surface, Nat. Phys. **5**, 398 (2009).
[19] A. A. Taskin and Y. Ando, Quantum oscillations in a topological insulator $Bi_{1-x}Sb_x$, Phys. Rev. B **80**, 085303 (2009).
[20] D. X. Qu, Y. S. Hor, J. Xiong, R. J. Cava, and N. P. Ong, Quantum oscillations and hall anomaly of surface states in the topological insulator Bi_2Te_3, Science **329**, 821 (2010).
[21] J. G. Analytis, R. D. McDonald, S. C. Riggs, J. H. Chu, G. S. Boebinger, and I. R. Fisher, Two-dimensional surface state in the quantum limit of a topological insulator, Nat. Phys. **6**, 960 (2010).
[22] P. Cheng, C. Song, T. Zhang, Y. Zhang, Y. Wang, J. F. Jia *et al.*, Landau Quantization of Topological Surface States in Bi_2Se_3, Phys. Rev. Lett. **105**, 076801 (2010).
[23] Z. Ren, A. A. Taskin, S. Sasaki, K. Segawa, and Y. Ando, Large bulk resistivity and surface quantum oscillations in the topological insulator Bi_2Te_2Se, Phys. Rev. B **82**, 241306 (R) (2010).
[24] A. A. Taskin, S. Sasaki, K. Segawa, and Y. Ando, Manifestation of Topological Protection in Transport Properties of Epitaxial Bi_2Se_3 Thin Films, Phys. Rev. Lett. **109**, 066803 (2012).
[25] J. Chen, H. J. Qin, F. Yang, J. Liu, T. Guan, F. M. Qu *et al.*, Gate-Voltage Control of Chemical Potential and Weak Antilocalization in Bi_2Se_3, Phys. Rev. Lett. **105**, 176602 (2010).
[26] H.-Z. Lu, J. Shi, and S.-Q. Shen, Competition Between Weak Localization and Antilocalization in Topological Surface States, Phys. Rev. Lett. **107**, 076801 (2011).
[27] H.-T. He, G. Wang, T. Zhang, I. K. Sou, G. K. L. Wong, J.-N. Wang, H.-Z. Lu, S.-Q. Shen, and F.-C. Zhang, Impurity Effect on Weak Antilocalization in the Topological Insulator Bi_2Te_3, Phys. Rev. Lett. **106**, 166805 (2011).
[28] G. Tkachov and E. M. Hankiewicz, Weak antilocalization in hgte quantum wells and topological surface states: Massive versus massless Dirac fermions, Phys. Rev. B **84**, 035444 (2011).
[29] I. Garate and L. Glazman, Weak localization and antilocalization in topological insulator thin films with coherent bulk-surface coupling, Phys. Rev. B **86**, 035422 (2012).
[30] J. H. Bardarson and J. E. Moore, Quantum interference and Aharonov-Bohm oscillations in topological insulators, Rep. Prog. Phys. **76**, 056501 (2013).
[31] M. Sitte, A. Rosch, E. Altman, and L. Fritz, Topological Insulators in Magnetic Fields: Quantum Hall Effect and Edge Channels with a Nonquantized θ Term, Phys. Rev. Lett. **108**, 126807 (2012).
[32] X. Wang, Y. Du, S. Dou, and C. Zhang, Room Temperature Giant and Linear Magnetoresistance in Topological Insulator Bi_2Te_3 Nanosheets, Phys. Rev. Lett. **108**, 266806 (2012).
[33] H. Peng, K. Lai, D. Kong, S. Meister, Y. Chen, X. L. Qi, S. C. Zhang, Z. X. Shen, and Y. Cui, Aharonov-bohm interference in topological insulator nanoribbons, Nat. Mater. **9**, 225 (2010).
[34] Y. Zhang and A. Vishwanath, Anomalous Aharonov-Bohm Conductance Oscillations from Topological Insulator Surface States, Phys. Rev. Lett. **105**, 206601 (2010).
[35] J. H. Bardarson, P. W. Brouwer, and J. E. Moore, Aharonov-Bohm Oscillations in Disordered Topological Insulator Nanowires, Phys. Rev. Lett. **105**, 156803 (2010).
[36] Y. Xu, I. Miotkowski, C. Liu, J. Tian, H. Nam, N. Alidoust, J. Hu, C. K. Shih, M. Z. Hasan, and Y. P. Chen, Observation of topological surface state quantum Hall effect in an intrinsic three-dimensional topological insulator, Nat. Phys. **10**, 956 (2014).
[37] R. Yoshimi, A. Tsukazaki, Y. Kozuka, J. Falson, K. Takahashi, J. Checkelsky, N. Nagaosa, M. Kawasaki, and Y. Tokura, Quantum Hall effect on top and bottom surface states of topological insulator $(Bi_{1-x}Sb_x)_2Te_3$ films, Nat. Commun. **6**, 6627 (2015).
[38] Y. S. Fu, M. Kawamura, K. Igarashi, H. Takagi, T. Hanaguri, and T. Sasagawa, Imaging the two-component nature of Dirac-Landau levels in the topological surface state of Bi_2Se_3, Nat. Phys. **10**, 815 (2014).
[39] R. Ilan, F. de Juan, and J. E. Moore, Spin-Based Mach-Zehnder Interferometry in Topological Insulator $p-n$ Junctions, Phys. Rev. Lett. **115**, 096802 (2015).
[40] S.-B. Zhang, H.-Z. Lu, and S.-Q. Shen, Edge states and integer quantum Hall effect in topological insulator thin films, Sci. Rep. **5**, 13277 (2015).
[41] Y. Xu, I. Miotkowski, and Y. P. Chen, Quantum transport of two-species Dirac fermions in dual-gated three-dimensional topological insulators, Nat. Commun. **7**, 11434 (2016).
[42] N. H. Tu, Y. Tanabe, Y. Satake, K. K. Huynh, and K. Tanigaki, In-plane topological pn junction in the three-dimensional topological insulator $Bi_{2-x}Sb_xTe_{3-y}Se_y$, Nat. Commun. **7**, 13763 (2016).
[43] P. Burset, B. Lu, G. Tkachov, Y. Tanaka, E. M. Hankiewicz, and B. Trauzettel, Superconducting proximity effect in

three-dimensional topological insulators in the presence of a magnetic field, Phys. Rev. B **92**, 205424 (2015).
[44] A. Taskin, H. F. Legg, F. Yang, S. Sasaki, Y. Kanai, K. Matsumoto, A. Rosch, and Y. Ando, Planar Hall effect from the surface of topological insulators, Nat. Commun. **8**, 1340 (2017).
[45] V. Dziom, A. Shuvaev, A. Pimenov, G. Astakhov, C. Ames, K. Bendias *et al.*, Observation of the universal magnetoelectric effect in a 3D topological insulator, Nat. Commun. **8**, 15197 (2017).
[46] P. He, S. S.-L. Zhang, D. Zhu, Y. Liu, Y. Wang, J. Yu, G. Vignale, and H. Yang, Bilinear magnetoelectric resistance as a probe of three-dimensional spin texture in topological surface states, Nat. Phys. **14**, 495 (2018).
[47] S.-B. Zhang and B. Trauzettel, Perfect Crossed Andreev Reflection in Dirac Hybrid Junctions in the Quantum Hall Regime, Phys. Rev. Lett. **122**, 257701 (2019).
[48] A. Assouline, C. Feuillet-Palma, N. Bergeal, T. Zhang, A. Mottaghizadeh, A. Zimmers *et al.*, Spin-orbit induced phase-shift in Bi_2Se_3 Josephson junctions, Nat. Commun. **10**, 126 (2019).
[49] H. Wu, P. Zhang, P. Deng, Q. Lan, Q. Pan, S. A. Razavi *et al.*, Room-Temperature Spin-Orbit Torque from Topological Surface States, Phys. Rev. Lett. **123**, 207205 (2019).
[50] S.-H. Zheng, H.-J. Duan, J.-K. Wang, J.-Y. Li, M.-X. Deng, and R.-Q. Wang, Origin of planar Hall effect on the surface of topological insulators: Tilt of Dirac cone by an in-plane magnetic field, Phys. Rev. B **101**, 041408(R) (2020).
[51] A. Dyrdał, J. Barnaś, and A. Fert, Spin-Momentum-Locking Inhomogeneities as a Source of Bilinear Magnetoresistance in Topological Insulators, Phys. Rev. Lett. **124**, 046802 (2020).
[52] A. Sulaev, M. Zeng, S.-Q. Shen, S. K. Cho, W. G. Zhu, Y. P. Feng, S. V. Eremeev, Y. Kawazoe, L. Shen, and L. Wang, Electrically tunable in-plane anisotropic magnetoresistance in topological insulator $BiSbTeSe_2$ nanodevices, Nano Lett. **15**, 2061 (2015).
[53] Unpublished results from the Molenkamp Lab.
[54] W.-Y. Shan, H.-Z. Lu, and S.-Q. Shen, Effective continuous model for surface states and thin films of three-dimensional topological insulators, New J. Phys. **12**, 043048 (2010).
[55] C.-X. Liu, X.-L. Qi, H. J. Zhang, X. Dai, Z. Fang, and S.-C. Zhang, Model hamiltonian for topological insulators, Phys. Rev. B **82**, 045122 (2010).
[56] A. Jost, M. Bendias, J. Böttcher, E. Hankiewicz, C. Brüne, H. Buhmann *et al.*, Electron–hole asymmetry of the topological surface states in strained HgTe, Proc. Natl. Acad. Sci. U.S.A. **114**, 3381 (2017).
[57] See Supplemental Material http://link.aps.org/supplemental/10.1103/PhysRevLett.127.076601 for details, which includes Refs. [54,58–64].
[58] M. I. Katsnelson, K. S. Novoselov, and A. K. Geim, Chiral tunnelling and the Klein paradox in graphene, Nat. Phys. **2**, 620 (2006).
[59] E. G. Novik, A. Pfeuffer-Jeschke, T. Jungwirth, V. Latussek, C. R. Becker, G. Landwehr, H. Buhmann, and L. W. Molenkamp, Band structure of semimagnetic $Hg_{1-y}Mn_yTe$ quantum wells, Phys. Rev. B **72**, 035321 (2005).
[60] M. Cardona, N. E. Christensen, and G. Fasol, Terms Linear in k in the Band Structure of Zinc-Blende-Type Semiconductors, Phys. Rev. Lett. **56**, 2831 (1986).
[61] L. Fu, Hexagonal Warping Effects in the Surface States of the Topological Insulator Bi_2Te_3, Phys. Rev. Lett. **103**, 266801 (2009).
[62] S.-B. Zhang, H.-Z. Lu, and S.-Q. Shen, Linear magnetoconductivity in an intrinsic topological Weyl semimetal, New J. Phys. **18**, 053039 (2016).
[63] V. H. Nguyen and J.-C. Charlier, Klein tunneling and electron optics in Dirac-Weyl fermion systems with tilted energy dispersion, Phys. Rev. B **97**, 235113 (2018).
[64] A. Wolos, S. Szyszko, A. Drabinska, M. Kaminska, S. G. Strzelecka, A. Hruban *et al.*, *g*-factors of conduction electrons and holes in Bi_2Se_3 three-dimensional topological insulator, Phys. Rev. B **93**, 155114 (2016).
[65] In a more elaborate model, we may include the warping effect of surface states. However, using realistic parameters for Bi-based topological insulators, we find that the influence of the warping effect on our main results is ignorable [57].
[66] We note, however, that the main results discussed below are not restricted to this condition.
[67] The local potential creates a Fermi-surface mismatch at the interfaces. This allows us to properly use the scattering approach to solve the transport problem, as discussed in Ref. [68].
[68] D. Breunig, S.-B. Zhang, B. Trauzettel, and T. M. Klapwijk, Directional electron-filtering at a superconductor-semiconductor interface, Phys. Rev. B **103**, 165414 (2021).
[69] A. Banerjee, A. Sundaresh, S. Biswas, R. Ganesan, D. Sen, and P. S. Anil Kumar, Topological insulator n-p-n junctions in a magnetic field, Nanoscale **11**, 5317 (2019).
[70] In the absence of tilting, $t_x = t_y = 0$, Eq. (7) reduces to a formula related to the transmission through npn junctions in graphene [58].
[71] We may look at the system as a Fabry-Péroit resonator between two interfaces. An electron can circulate in the resonator. In one round trip, the electron acquires a phase shift $(\tilde{k}_+^B - \tilde{k}_-^B)L$.
[72] Fluctuations of L in y-direction and spatial variation of V_0 may effectively lead to a fluctuation $\delta n(k_y)$ of the numbers $n(k_y)$ for resonant modes. However, if the fluctuation is small, $\delta n(k_y)/n(k_y) \ll 1$, such that the numbers for resonant modes are limited to a moderate range of integers, then a net effect of the superresonance can be observed.
[73] Note that this is only true when $|V_0| \gg |E_F|$. When this condition is softened, the value $\Delta G_{\rm osc}/G_{\rm max}$ becomes smaller.
[74] Using Eqs. (11) and (13), B_c could be estimated as $\min(2/|\gamma|, 2\pi n_c' F/|mE_F L|)vF/(g\mu_B)$ with $F = \sqrt{v[v - V_0 L/\pi(n_c+1)]}$.
[75] S. Wiedmann, A. Jost, B. Fauqué, J. van Dijk, M. J. Meijer, T. Khouri *et al.*, Anisotropic and strong negative magnetoresistance in the three-dimensional topological insulator Bi_2Se_3, Phys. Rev. B **94**, 081302(R) (2016).
[76] S. Hart, H. Ren, M. Kosowsky, G. Ben-Shach, P. Leubner, C. Brüne, H. Buhmann, L. W. Molenkamp, B. I. Halperin, and A. Yacoby, Controlled finite momentum pairing and

spatially varying order parameter in proximitized HgTe quantum wells, Nat. Phys. **13**, 87 (2017).

[77] D. Rakhmilevich, F. Wang, W. Zhao, M. H. W. Chan, J. S. Moodera, C. Liu, and C.-Z. Chang, Unconventional planar Hall effect in exchange-coupled topological insulator–ferromagnetic insulator heterostructures, Phys. Rev. B **98**, 094404 (2018).

[78] B. Wu, X.-C. Pan, W. Wu, F. Fei, B. Chen, Q. Liu, H. Bu, L. Cao, F. Song, and B. Wang, Oscillating planar Hall response in bulk crystal of topological insulator Sn doped $Bi_{1.1}Sb_{0.9}Te_2S$, Appl. Phys. Lett. **113**, 011902 (2018).

[79] In HgTe, the phase coherence length can be larger than 5 μm at temperature $T = 40$ mK [80], and the bulk energy gap can be larger than 50 meV [81,82]. To the best of our knowledge, the in-plane g-factor of topological surface states in HgTe is still not known experimentally. However, we notice that in a related 2D system, the quantum spin Hall phase of HgTe quantum wells, the 2D electron gas has an in-plane g-factor of 20.5 [83]. We may expect a similar g-factor for the surface states.

[80] J. Ziegler, R. Kozlovsky, C. Gorini, M. H. Liu, S. Weishäupl, F. Maier *et al.*, Probing spin helical surface states in topological HgTe nanowires, Phys. Rev. B **97**, 035157 (2018).

[81] S.-C. Wu, B. Yan, and C. Felser, Ab initio study of topological surface states of strained HgTe, Europhys. Lett. **107**, 57006 (2014).

[82] T. Rauch, S. Achilles, J. Henk, and I. Mertig, Spin Chirality Tuning and Topological Semimetals in Strained $HgTe_xS_{1-x}$, Phys. Rev. Lett. **114**, 236805 (2015).

[83] M. König, H. Buhmann, L. W. Molenkamp, T. Hughes, C.-X. Liu, X.-L. Qi, and S.-C. Zhang, The quantum spin hall effect: Theory and experiment, J. Phys. Soc. Jpn. **77**, 031007 (2008).

[84] For larger parameters V_0L, v, g or $4m^2 + \gamma^2$, we may expect the oscillations to appear in smaller fields.